Chinese Journal of Chemical Engineering 53 (2023) 73–82

Contents lists available at ScienceDirect

Chinese Journal of Chemical Engineering

journal homepage: www.elsevier.com/locate/CJChE

Full Length Article

A self-healing and conductive ionic hydrogel based on polysaccharides for flexible sensors

Yufei Wang, Zihao Chen, Rui Chen, Jie Wei *

Beijing Engineering Research Center for the Synthesis and Applications of Waterborne Polymers, Beijing 100029, China
Key Laboratory of Carbon Fibers and Functional Polymers, Ministry of Education, Beijing 100029, China
College of Materials Science and Engineering, Beijing University of Chemical Technology, Beijing 100029, China

ARTICLE INFO

Article history:
Received 29 September 2021
Received in revised form 13 February 2022
Accepted 20 February 2022
Available online 13 April 2022

Keywords:
Hydrogel
Self-healing
Conductivity
Polysaccharide
Flexible sensor

ABSTRACT

In this study, we proposed a self-healing conductive hydrogel based on polysaccharides and Li^+ to serve as flexible sensors. At first, the oxidized sodium alginate (OSA) was obtained through the oxidation reaction of sodium alginate (SA). Then OSA, carboxymethyl chitosan (CMC), and agarose (AGO) were dissolved in LiCl solution, respectively. Finally, the hydrogel was obtained through heating, mixing, and cooling processes. Because of the Schiff base structure and hydrogen bonding, the hydrogel demonstrates good mechanical and self-healing properties. The presence of Li^+ provides good conductivity for the hydrogel. In addition, we demonstrated the application of the hydrogel as the flexible sensors. It can perceive the process of pressing Morse code with the index finger as a pressure sensor and monitor sliding movement of the thumb as the strain sensor to browse the web with the mobile phone. Thus, the self-healing conductive hydrogel may have potential applications in flexible wearable sensors.

1. Introduction

Hydrogels are cross-linked three-dimensional network polymer materials with good hydrophilicity, which can absorb a large amount of water and have a certain swelling rate [1,2]. In recent years, hydrogels with different functionality have been successfully prepared [3,4]. By designing polymer molecules and doped materials, hydrogels can be endowed with various characteristics, such as injectable, transparent, self-healing, conductive, and stimulus-responsive properties [5–9]. Among them, self-healing and conductive properties have received extensive attention, and hydrogels that combine both self-healing and conductive properties demonstrate great advantages, which have potential applications in the fields of the repairable circuit, wearable electronic devices, electronic skin, multi-functional sensors, metal ion detection, tissue engineering, and biomedicine [10–18]. Cheap polysaccharides with good biocompatibility and antibacterial properties, include sodium alginate, gelatin, chitosan, cellulose, hyaluronic acid, agar, and so on, which are ideal materials to prepare hydrogels. However, hydrogels fabricated from polysaccharides usually have poor mechanical properties, which greatly limits their applications. However, some hydrogels fabricated by synthetic polymers or double-network hydrogels prepared by combining polysaccharide macromolecules and synthetic polymers have excellent mechanical properties, but both the preparation process and biocompatibility need to be improved [19–22].

As a polysaccharide, agarose can form a double-helix structural network after heating and cooling processes, and the agarose network can be combined with other polymer networks through physical entanglement and hydrogen bonding, which can significantly improve the mechanical properties of the hydrogels [23–24]. Therefore, by adding agarose into polysaccharide hydrogels may improve their mechanical performance.

Self-healing properties can prevent materials from aging and wear and can effectively improve their service life, which have been widely researched and employed [25,26]. Self-healing hydrogels usually have reversible chemical bonds or interactions [27]. Under external stimuli, these chemical bonds or interactions will be broken, and materials will exhibit macroscopical scratches or breaks. Under certain conditions, when the damaged surfaces come into contact with each other, these chemical bonds or interactions will be reconstructed, and materials will exhibit self-healing behavior [28,29]. In regard to the self-healing mechanism, self-healing hydrogels can be simply divided into hydrogels with the reversible covalent bonds and those with the supramolecular

* Corresponding author.
E-mail address: weij@mail.buct.edu.cn (J. Wei).

https://doi.org/10.1016/j.cjche.2022.02.022
1004-9541/

interactions [30,31]. Reversible covalent bonding includes formation of imine bonds (Schiff base), acylhydrazone bonds, phenylboronic ester bonds, disulfide bonds, and Diels-Alder reaction [32–36]. Supramolecular interactions include formation of hydrogen bond, metal ion coordination bond, hydrophobic interaction, and host-guest interaction [37–40]. Hydrogels with different self-healing mechanisms have different self-healing efficiencies. Ambient conditions such as temperature and pH will also have a certain effect on self-healing properties [41,42].

Traditional hydrogels have very low conductivity because they absorb a lot of water, and their conductivity value does not meet the level suitable for applications [43]. In recent years, more and more hydrogels with excellent conductive properties have been successfully prepared, which can be simply divided with regard to their conductive mechanism into conductive polymers and doped conductive materials [44–46]. Conductive polymers include polyaniline, polypyrrole, polythiophene, and their derivatives [47–50]. Although conductive polymers have good conductive properties, lack in transparency limits their application [51]. Conductive materials that can be doped include graphene, carbon nanotubes, silver nanowires, and MXene, which are hardly improvable in terms of transparency and dispersion [52–56]. In addition, some ions from salts like NaCl and KCl can be introduced into hydrogels after dissolving them in water, though the conductivity still needs to be improved [57,58]. However, Li^+ has a small ionic radius, which is easy to migrate into the hydrogel network and endows higher conductivity as compared with other ions [59,60], so it may be used to prepare ionic hydrogels with high conductivity.

Recently, many excellent hydrogel sensors have been successfully prepared. For instance, Han *et al.* [61] reported a dual conductive network hydrogel based on carrageenan, polyacrylamide, and carbon nanotubes films, which possess highly conductive, self-healing, anti-freezing, and non-drying properties and can be used as strain sensors to detect biosignals in real time. Wang *et al.* [62] reported a double-layer hydrogel with asymmetrical adhesion, and self-powered properties, which provides new potential applications for wearable electronics. Zheng *et al.* [63] reported a self-healing and conductive hydrogel based on PVA-Borax and (±)-α-Thioctic acid-iron (III) (TA-Fe^{3+}), which can be used as a strain sensor to detect the movement of the body joints. However, the comprehensive performance of these hydrogel sensors in terms of mechanical properties, self-healing properties, and biocompatibility needs to be improved. In addition, in the selection of conductive materials, although dark-colored conductive filler materials have excellent conductive properties, they also have a certain impact on the aesthetics of the hydrogel [52,62]. Therefore, it is still a challenge to prepare a wearable hydrogel sensor with the above-mentioned excellent performance.

In this study, we propose a facile method for the fabrication of self-healing conductive hydrogel based on oxidized sodium alginate (OSA), carboxymethyl chitosan (CMC), agarose (AGO), and LiCl. Through the oxidation treatment of sodium alginate (SA), we provided OSA with aldehyde groups. Schiff base structure can be formed with OSA and CMC, which acts not only as a cross-linking point of the hydrogel network but also endows the hydrogel with self-healing property. Simultaneously, we introduced AGO into the hydrogel interacting with other components through physical entanglement and hydrogen bonding. Accordingly, AGO could improve mechanical properties of the hydrogel. OSA, CMC, and AGO are simply modified natural polysaccharide polymers, hence choosing them as raw materials could endow the hydrogel with excellent biocompatibility. In addition, we used LiCl aqueous solution to prepare the hydrogel. There are a large number of Li^+ and Cl^- in the hydrogel that can move freely, so the hydrogel possesses electrical conductivity. We systematically studied both self-healing and conductive properties of the hydrogel. The macroscopic self-healing and rheological tests were used to measure self-healing property of the hydrogel, whereas the conductivity of the hydrogel was demonstrated by the LED strip lighting. Moreover, the conductivity of the hydrogel may be affected by the compression ratio and bending angle. Changes in these conditions may affect the migration of conductive ions in the hydrogel and cause resistance changes. As a result, we have designed the flexible sensors as the pressure sensor and the strain sensor respectively, which can be used to perceive the information from the Morse code pressed by a finger and to detect the sliding movement of a finger to browse the web with the mobile phone. This work proposes a novel structure of self-healing conductive hydrogel, which provides new potential applications for multifunctional sensors, as well as a wearable device.

2. Materials and Methods

2.1. Materials

Sodium alginate (SA, 99%), sodium periodate ($NaIO_4$, 99%), ethylene glycol (EG, 99%), sodium bicarbonate ($NaHCO_3$, 99%), standardized sodium thiosulphate solution (0.01 $mol \cdot L^{-1}$), and starch indicator (0.2% in water) were purchased from Aladdin (Shanghai, China). Carboxymethyl Chitosan (CMC, 99%, degree of substitution 80%), agarose (AGO, 98%), lithium chloride (LiCl, 99%), methylene blue (99%), potassium iodide (KI, 99%), were purchased from Shanghai Macklin Biochemical Co., Ltd. All of the chemicals were used as received without further purification.

2.2. Preparation of oxidized sodium alginate (OSA)

SA (5 g) and ethanol (25 ml) were mixed together under stirring to obtain the suspension. Then, $NaIO_4$ (2.67 g) was dissolved in 25 ml distilled water. Afterwards, $NaIO_4$ solution was added into the suspension, and the mixture was stirred in the dark at 25 °C for 4 h. Ethylene glycol (5 ml) was added into the mixture that was continuously stirred for 30 min to terminate the reaction. Then, the mixture was poured into a dialysis bag (cut off M_w = 7500) dialyzed against deionized water for 3 d with changing water every 6 hours. Finally, OSA was obtained by freeze-drying method. The oxidation degree of OSA was determined by iodometry.

2.3. Preparation of OSA-CMC-AGO/Li^+ hydrogel

OSA (5 g) and CMC (5 g) were dissolved in 95 ml LiCl solution (5%) at 60 °C, respectively. AGO (5 g) was added into 95 ml LiCl solution (5%) under stirring at 95 °C to obtain the transparent solution and cooled to 60 °C. Consequently, the solution of OSA (5 ml), CMC (20 ml), and AGO (10 ml) were mixed and stirred quickly, and then the hydrogel precursor solution was poured into a special mold and left for 48 h at room temperature to obtain OSA-CMC-AGO/Li^+ hydrogel. The control group set contained different AGO content at 0, 5, 10, 15 ml and referred to as OSA-CMC/Li^+, OSA-CMC-AGO1/Li^+, OSA-CMC-AGO2/Li^+, and OSA-CMC-AGO3/Li^+, respectively.

2.4. Characterization

FTIR tests: functional group characteristic peak of the raw materials and hydrogels were characterized by FTIR spectroscopy (Nicolet 6700) at room temperature.

Water content and swelling ratio: the gravimetric method was used to test the water content and swelling ratio of the hydrogels. Different hydrogels with the same shape and size were weighed.

Then the hydrogels were weighed after freeze-drying. The water content ratio was calculated using the following equation:

$$\text{Water content} = \frac{W_t - W_d}{W_t} \times 100\%$$

where W_t is the mass of hydrogel and W_d is the mass of the dried hydrogel. The measurement was performed three times and the mean value was used.

The swelling ratio was tested using a similar method. The different hydrogels with the same shape and size were weighed after freeze-dried. Then the hydrogels were fully immersed in deionized water for 2 d. Finally, the swollen hydrogels were weighed after wiped excess water on the surface with filter paper. The swelling ratio was calculated using the following equation:

$$\text{Swelling ratio} = \frac{W_t' - W_d}{W_d} \times 100\%$$

where W_t' is the mass of swollen hydrogel and W_d is the mass of the dried hydrogel. The measurement was performed three times and the mean value was used.

Mechanical tests: mechanical properties of hydrogels were measured by universal testing mechanical machine (INSTRON 5567). Hydrogel samples with the height of 10 mm and diameter of 10 mm were prepared. Then, the compression properties of hydrogels were tested with the operating speed of 5 mm·min^{-1} at room temperature.

SEM tests: the internal structure of hydrogels was observed by SEM (JEOL JSM-7800F). The hydrogels were freeze-dried and fractured with the liquid nitrogen to observe the cross-section.

Rheological tests: the hydrogels were tested with the rheometer (Discovery HR1). The storage modulus (G') and loss modulus (G'') of hydrogels were test under strain sweep and alternating strain modes.

Conductivity tests: electrical properties of hydrogels were measured with the electrochemical workstation (CHI 660E CHENHUA). The conductivity was calculated using the following equation:

$$\sigma = \frac{L}{RS}$$

where σ represents the conductivity, R represents the resistance, L represents the electrode spacing, and S represents the hydrogel cross-sectional area.

3. Results and Discussion

3.1. Preparation and characterization of OSA-CMC-AGO/Li$^+$ hydrogel

OSA-CMC-AGO/Li$^+$ hydrogel was synthesized through the simple method. Fig. 1(a) illustrates schematic diagram of the synthesis route for the hydrogel. Three groups of OSA, CMC and, AGO were dissolved in aqueous solution of LiCl, then heated and mixed together, and finally allowed for cooling at room temperature to obtain OSA-CMC-AGO/Li$^+$ hydrogel. The aldehyde group in OSA and the amino group in CMC could form reversible Schiff base structures, which not only provide the basis for mechanical properties as the cross-linking point of the hydrogel network, but also endow the hydrogel with self-healing property. The molecular structures of OSA, CMC, and Schiff base are shown in Fig. 1(b). Moreover, AGO was formed the linear chain structure and dissolved in water under heating further forming the helix structure after cooling. Accordingly, AGO network could be combined with OSA-CMC network through physical entanglement and hydrogen bonding, which may improve the mechanical properties of the hydrogel.

Fig. 2 shows the FTIR spectra of the polysaccharides and hydrogel. The spectra of OSA exhibit the C=O stretching vibration peak at 1735 cm^{-1} as shown in Fig. 2(a), which confirms the presence of aldehyde groups. The oxidation degree of OSA as measured by the iodometry was found to be about 36.9%. In Fig. 2(b), the peak at 3440 cm^{-1} of CMC has been attributed to the O—H and N—H stretching vibration, the peak at 1608 cm^{-1} of CMC has been attributed to the asymmetric stretching vibration of carboxyl group and N—H bending vibration, and the peak at 1315 cm^{-1} has been attributed to the C—N stretching vibration, that is the characteristic peak of the amine group. In the hydrogel spectra, the peak at 1735 cm^{-1} of aldehyde group disappears, and the peak at 1315 cm^{-1} of C—N stretching vibration became weaker. Furthermore, the O—H and N—H stretching vibration peak red-shifted to 3390 cm^{-1}. Correspondingly, this confirms the reduction of aldehyde groups and amino groups and the formation of Schiff base structure, the peak at 1618 cm^{-1} includes the C=N stretching vibration peak. After the introduction of AGO, the characteristic peaks of the hydrogel do not change much, indicating that AGO does not affect the formation of Schiff base structure as shown in Fig. S1 (in Supplementary Material).

In the series of prepared hydrogels, the water content reaches to about 88% as shown in Fig. 3(a). After the introduction of AGO, the swelling ratio of the hydrogel decreases, and the swelling ratio of AGO hydrogel has the smallest value, as shown in Fig. 3(b). This is because AGO helix structure forming a dense network with little water swelling, while OSA-CMC network is relatively soft and can absorb a lot of water. Therefore, OSA-CMC network has a higher swelling ratio than AGO network. Fig. 3(c) shows the compression stress–strain curves of the hydrogels. It can be seen that the hydrogel becomes tougher and stronger as the content of AGO increases, and this is accompanied by the decrease in maximum compressive strain. At the same time, the compression modulus of the hydrogel also increases with the increasing content of AGO, as shown in Fig. S2. This further denotes both softness and flexibility of OSA-CMC network and toughness of AGO network, and also denotes the AGO to be capable enhancing the self-healing network of OSA-CMC. Therefore, for the subsequent applicability test we choose OSA-CMC-AGO2/Li$^+$ hydrogel with regard to its toughness and strength. The compression cycle stress–strain curve of OSA-CMC-AGO2/Li$^+$ hydrogel was tested and shown in Fig. 3(d). Rather large hysteresis loop appears in the first compression cycle which confirms the effective energy dissipation of the hydrogel. Before the first compression, the hydrogel internal network is in an initial stable state. When compressed for the first time, the hydrogel is suddenly subjected to external force, and the internal macromolecular chains slip between them. In addition, the dynamic Schiff base structure and intermolecular hydrogen bonds in the hydrogel network will also be partially broken to adapt to the change of external force under the action of external force. The recovery time of molecular chains and chemical bonds is slow when the external force is withdrawn, so the hydrogel exhibits remarkably large energy loss during the first compression. In the subsequent cyclic compression, the hydrogel network has adapted to this cyclic external force change, so it exhibits smaller energy loss. The hysteresis loop becomes much smaller in the second cycle. Moreover, the stress–strain curve of the hydrogel changes slightly after many cycles, which confirms the structural integrity and fatigue resistance of the hydrogel.

Internal morphologies of the hydrogels were observed by SEM, as shown in Fig. 4. It can be seen that the three freeze-dried hydrogels all have a porous microstructure. OSA-CMC/Li$^+$ hydrogel network (Fig. 4(a)) demonstrates large pores, whereas AGO/Li$^+$ hydrogel network (Fig. 4(c)) is denser with smaller pores. That is because of the tight integration of AGO double helix structure, which also endows hydrogels with excellent mechanical strength.

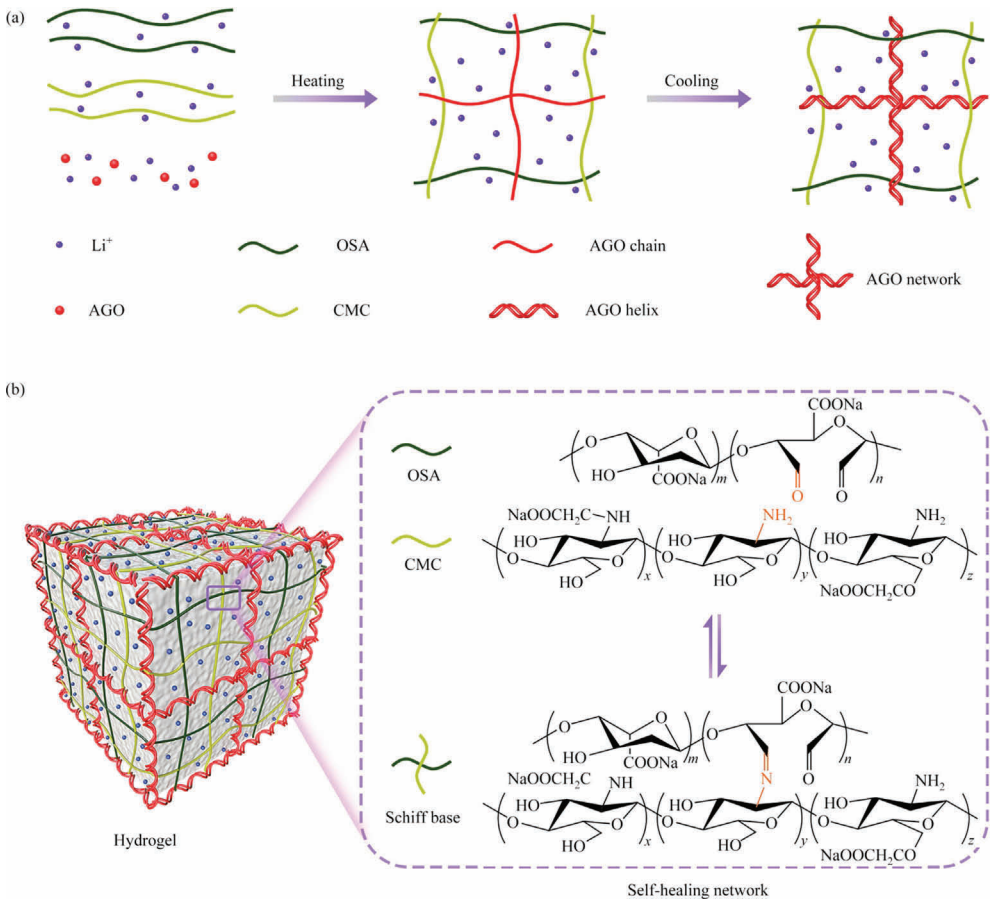

Fig. 1. (a) Schematic diagram of the synthesis route for OSA-CMC-AGO/Li^+ hydrogel. (b) Self-healing network of OSA-CMC-AGO/Li^+ hydrogel.

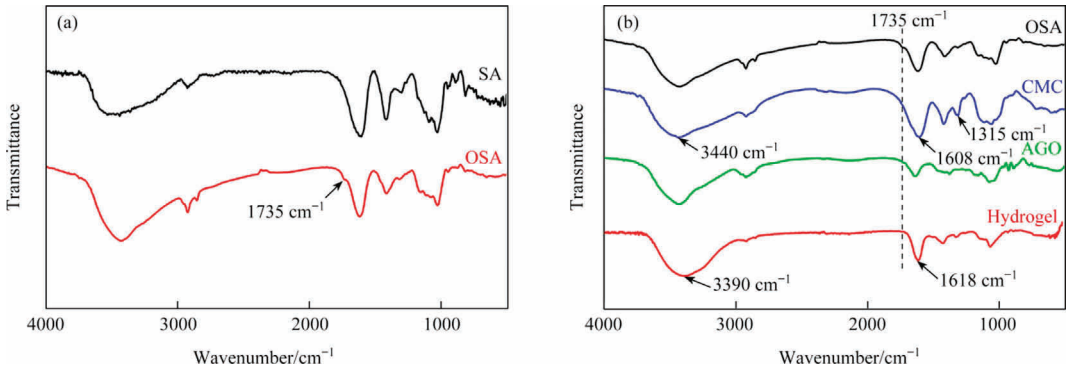

Fig. 2. FTIR spectra of (a) SA, OSA, (b) OSA, CMC, AGO, and the hydrogel.

The continuous holes in the OSA-CMC-AGO hydrogel network (Fig. 4(b)) indicate that both AGO and OSA-CMC networks are well combined without agglomeration. In addition, the pore structure of the hydrogel may allow Li^+ to migrate freely inside the hydrogel, which makes it possess a certain degree of conductivity.

3.2. Self-healing and conductive properties of OSA-CMC-AGO/Li^+ hydrogel

Fig. 5 illustrates self-healing properties of the hydrogels. Macroscopic self-healing of the hydrogel is shown in Fig. 5(a). At first, heated and mixed hydrogel precursor solution was poured into the designated mold, and 3 ml of methylene blue solution was added to one of the hydrogels for dyeing. The hydrogel was obtained after cooling. The obtained hydrogel was cut into two pieces allowed to touch together, at room temperature. Self-healing of the hydrogel was basically completed after 24 h. Fig S4 shows the microstructure at incision region of the hydrogel before and after self-healing, it can be seen that the incision region of the hydrogel basically healed after 24 h. The self-healing efficiency of the hydrogel is about 90% after 24 h by comparing the compressive stress–strain curves of the hydrogel before and after self-healing, as shown in Fig S5. To further examine self-healing properties of the hydrogels, we conducted rheological tests as shown in Fig. 5(b) and (c). It can be seen that the storage modulus (G') and loss modulus (G'') of the hydrogels both exhibit alternating changes under 5% and 800% strain. Modulus G' is greater than G'' of the hydrogels under 5% strain, which presents the solid state. The

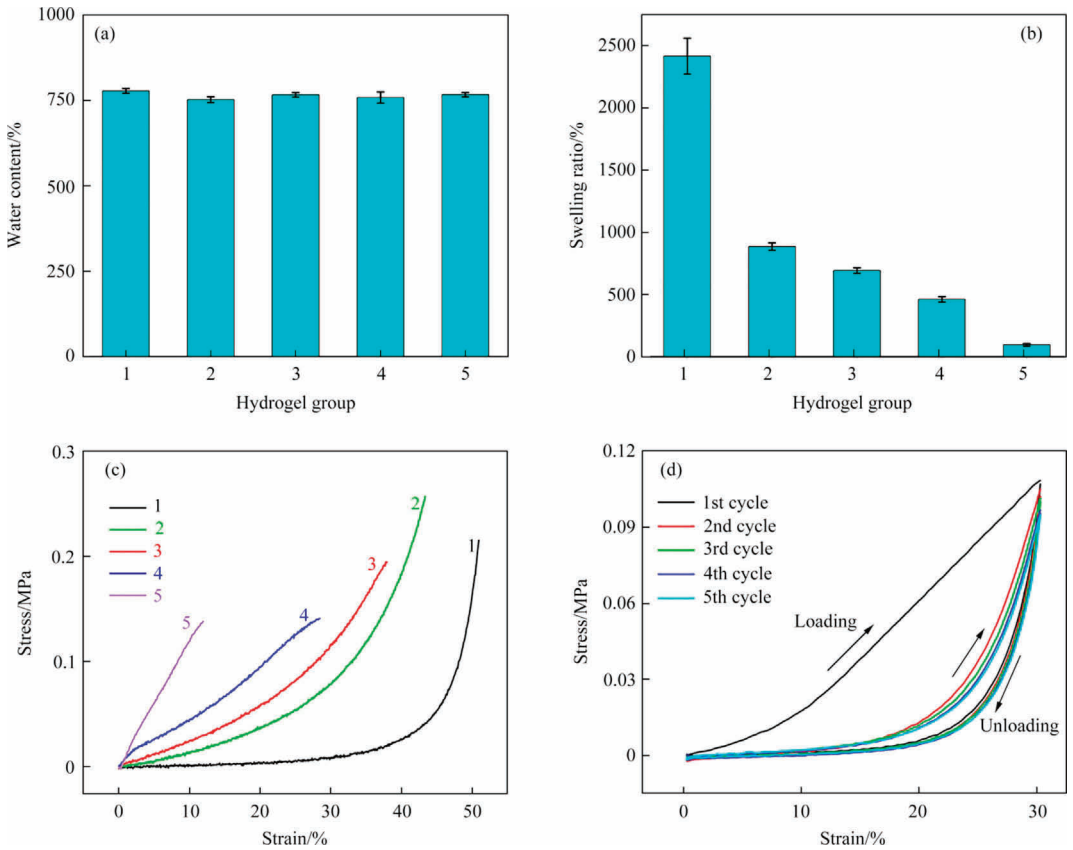

Fig. 3. (a) Water content, (b) swelling ratio, and (c) compression stress–strain curves of different hydrogel groups. (1: OSA-CMC/Li^+ 2: OSA-CMC-AGO1/Li^+ 3: OSA-CMC-AGO2/Li^+ 4: OSA-CMC-AGO3/Li^+ 5: AGO/Li^+.) (d) Compression cycle stress–strain curve of OSA-CMC-AGO2/Li^+ hydrogel.

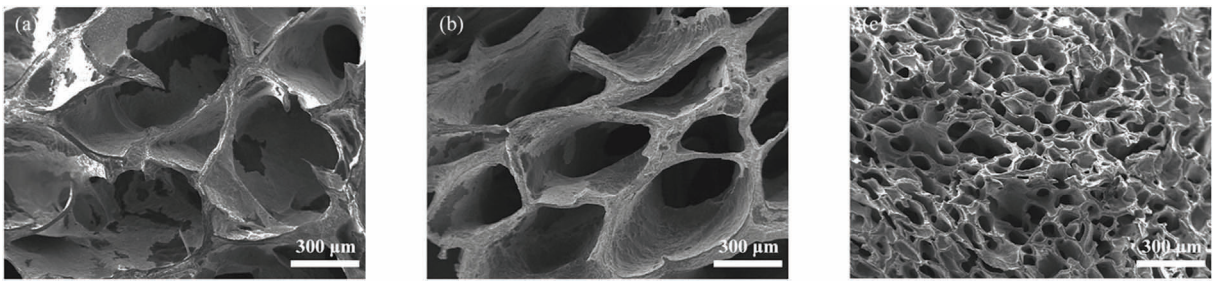

Fig. 4. SEM images of (a) OSA-CMC/Li^+, (b) OSA-CMC-AGO/Li^+, and (c) AGO/Li^+ hydrogels.

G'' is greater than G' of the hydrogels under 800% strain, which represents the liquid state. The cyclic change with 200 s period shows good self-healing performance of hydrogels. Moreover, in general the modulus of OSA-CMC-AGO/Li^+ is greater than the modulus of OSA-CMC/Li^+, which proves the introduction of AGO could enhance mechanical properties of the hydrogels.

We further demonstrated the self-healing and conductive properties of the hydrogel with the LED strip as shown in Fig. 6(a) and (b). The hydrogel precursor solution was poured into a mold to obtain the cuboid hydrogel (length 50 mm, width 10 mm, and height 10 mm) after cooling. We have designed the circuit that contains the hydrogel and the LED strip with a rated voltage of 12 V. When the circuit was turned off, it was in the open-circuit state, and the LED strip did not emit light. After connecting the hydrogel to the circuit, the LED strip starts emitting light. Then the hydrogel was cut, and the circuit was in the open-circuit state again. The LED strip did not emit light. Then, two pieces of the hydrogel were contacted, and reconnected to the circuit after completed self-healing. The LED strip appeared to glow again. It can be seen that this hydrogel has both good self-healing and conductive properties.

We tested the electrical conductivity of the hydrogels with different Li^+ concentrations, as shown in Fig. 6(c). As Li^+ concentration increases, the electrical conductivity of the hydrogel also tends to increase. When Li^+ is not added, the hydrogel has its relatively low conductivity (0.56 $S{\cdot}m^{-1}$), which is because of the sodium carboxylate structure of both OSA and CMC that could dissociate to $—COO^-$ and Na^+ in water as polyelectrolytes. The initial conductivity is not high due to Li^+ low content. When Li^+ concentration is 5%, the conductivity reaches 1.15 $S{\cdot}m^{-1}$. In addition, when the Li^+ concentration is higher than 5%, the conductivity of the hydrogel does not increase significantly as shown in Fig. S3. This may be due to the limitation in size of the hydrogel pores, OSA-CMC and AGO hydrogel network cannot allow more Li^+ to move freely. More importantly, we have also tested the resistance change of the hydrogel under compression and bending conditions. Fig. 6(d)

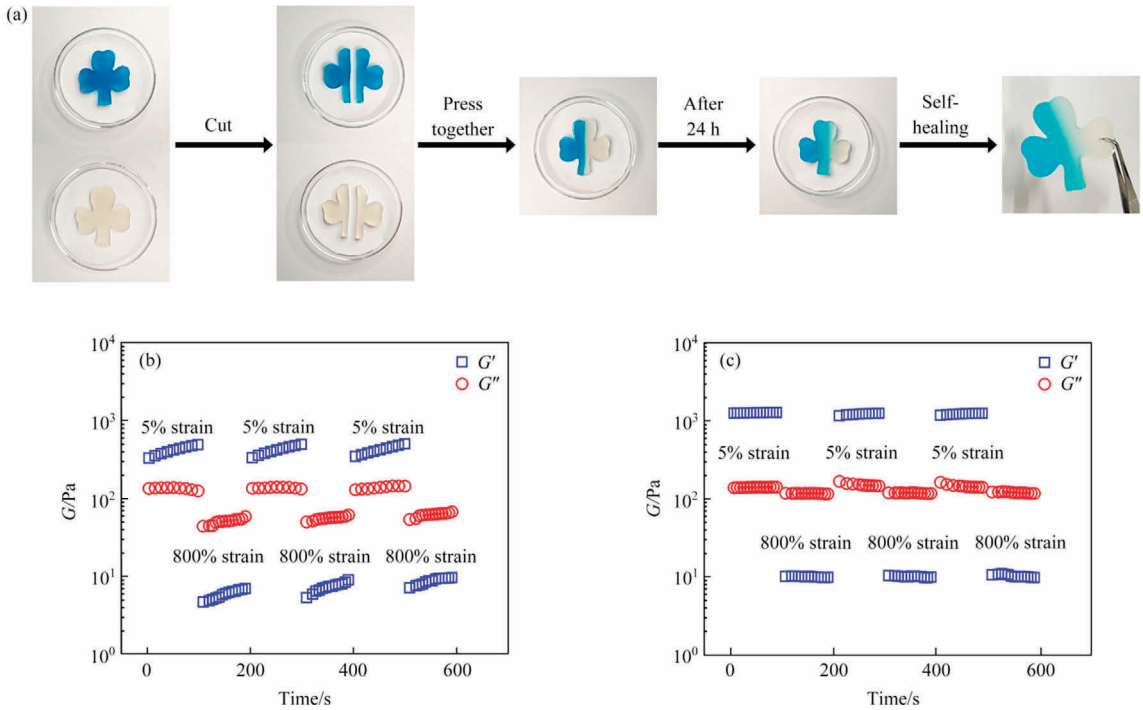

Fig. 5. (a) Self-healing property of OSA-CMC-AGO/Li^+ hydrogel. Rheological tests of (b) OSA-CMC/Li^+ and (c) OSA-CMC-AGO/Li^+ hydrogels.

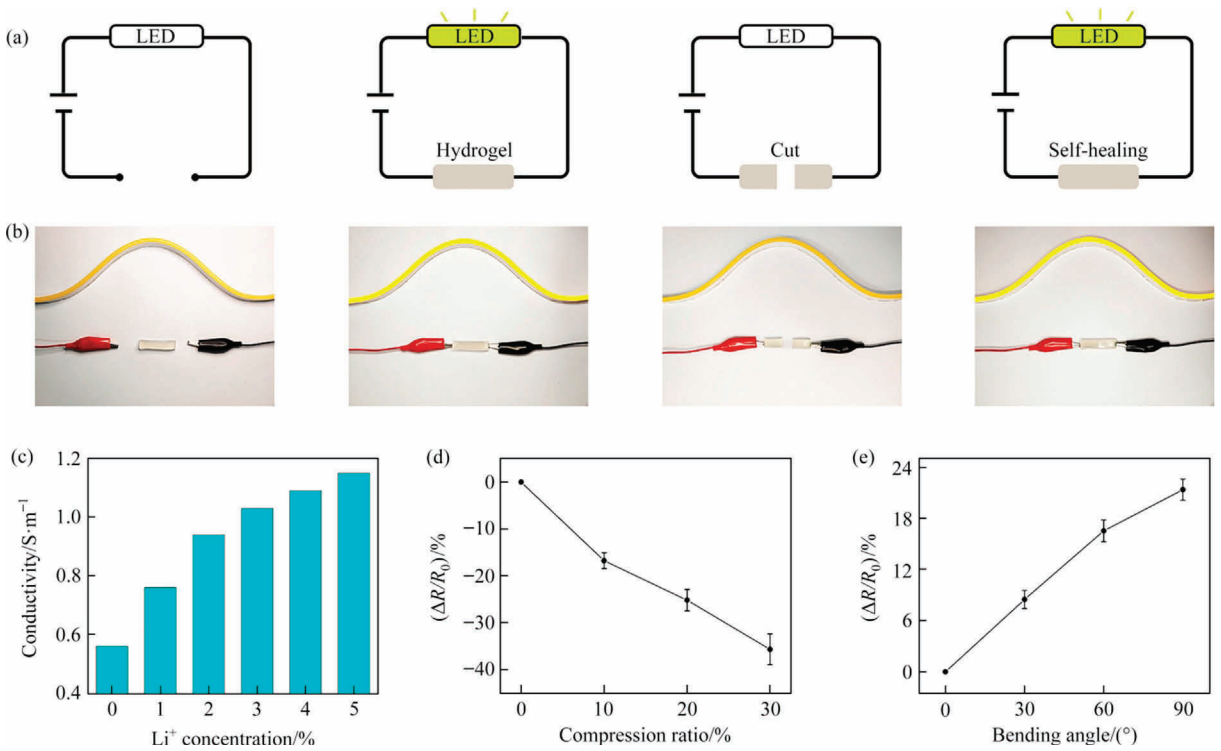

Fig. 6. (a) Schematic diagram of the circuit. (b) Conductivity of OSA-CMC-AGO/Li^+ hydrogel. (c) Conductivity of hydrogels with different Li^+ concentrations (0, 1%, 2%, 3%, 4% and 5%). (d) Resistance change rate of the hydrogel under different compression ratios at 0, 10%, 20%, and 30%. (e) Resistance change rate of the hydrogel under different angles at 0°, 30°, 60°, and 90°.

shows the resistance change rate of the hydrogel at the compression rates of 10%, 20%, and 30%. It can be seen that the hydrogel has obvious changes in resistance under different compression rates. Moreover, the resistance of the hydrogel under different bending angles (10°, 20°, and 30°) also demonstrate similar changes as shown in Fig. 6(e).

3.3. OSA-CMC-AGO/Li^+ hydrogel as the flexible sensors

3.3.1. The hydrogel as the pressure sensor by index finger

The hydrogel precursor solution was poured into a designated mold to obtain a cylindrical hydrogel (diameter 45 mm, height 10 mm). The metal sheets were stuck to both sides of the hydrogel

as the electrode and connected with wires to obtain the hydrogel-based pressure sensor, as shown in Fig. 7(a) and (b). Since the hydrogel is compressed during the pressing process, the distance between two electrodes becomes shorter, and the section becomes slightly larger, which reduces the resistance of the hydrogel. Therefore, the pressure action can be monitored according to the real-time resistance change rate of the hydrogel. The hydrogel pressure sensor can be used to perceive the pressure of the index finger, as shown in Fig. 8(a) and (b). Fig. 8(c) shows the resistance change rate of the hydrogel during the process of "long press" and "short press". The compression time can be clearly seen in this figure. Therefore, we designed a set of Morse codes corresponding to B, U, C, and T respectively, in which the dash means longer duration of pressing, and the dot means shorter press duration, as shown in Fig. 8(d). Correspondingly, the index finger pressure action can be converted into recordable and transmittable electrical signal through the real-time resistance change rate of the hydrogel. Fig. 8(e) shows the resistance change rate of the hydrogel in the process of pressing the Morse code, which can clearly distinguish the change of the press with longer duration and the press of shorter duration as well as the difference in the applied force each time the hand is pressed, so the hydrogel could exhibit pretty good pressure sensor effect. The sensitivity of the hydrogel sensor is 1.15, and the response and recovery time of the hydrogel sensor

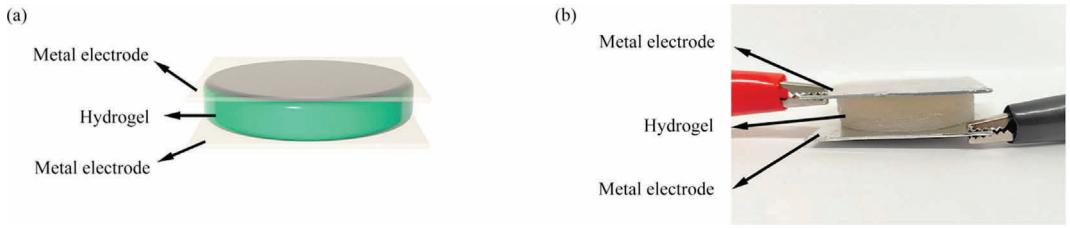

Fig. 7. (a) Structure of the hydrogel pressure sensor. (b) Photograph of the hydrogel pressure sensor.

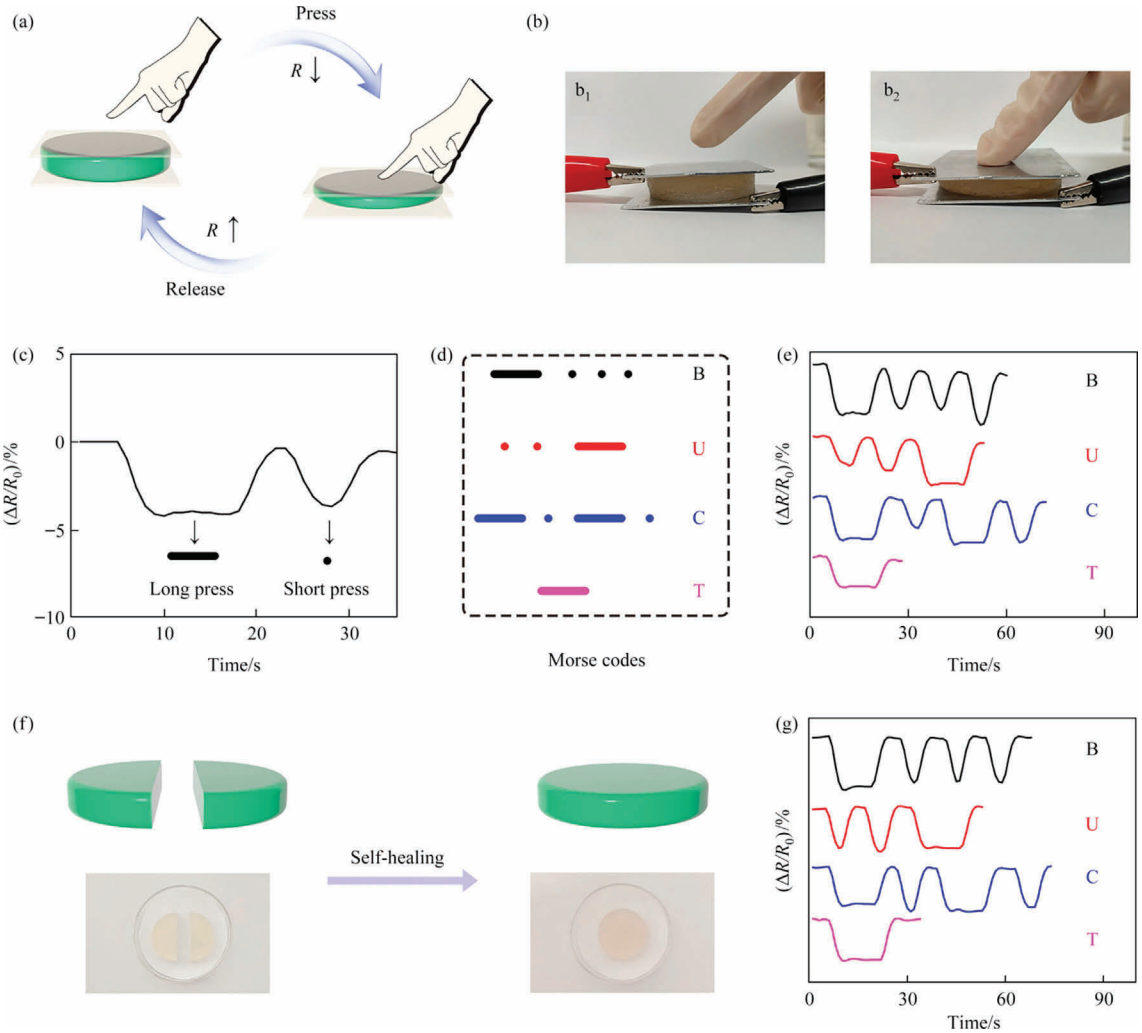

Fig. 8. (a) Schematic illustration of the hydrogel serving as the pressure sensor. (b) Photographs of the hydrogel serving as the pressure sensor. (b_1: initial state of the pressure sensor, b_2: compressed state of the pressure sensor.) (c) Resistance change rate of the hydrogel during the process of "long press" and "short press". (d) The Morse code of "B" "U" "C" "T". (e) Resistance change rate of the hydrogel during the process of pressing with the index finger. (f) Self-healing property of the pressure sensor. (g) Resistance change rate of the hydrogel during the process of pressing with the index finger after self-healing.

is 321 ms and 342 ms as shown in Fig S6. We also tested the resistance change rate of the hydrogel sensor under 30% compressive strain in 100 cycles. The hydrogel pressure sensor possesses certain stability, as shown in Fig. S7. Moreover, the hydrogel could continue to monitor the finger pressure serving as the pressure sensor after self-healing, as shown in Fig. 8(f) and (g).

3.3.2. The hydrogel as the strain sensor by thumb finger

Similarly, the hydrogel precursor solution was poured into the designated mold to obtain a cuboid hydrogel (length 50 mm, width 15 mm, and height 5 mm). The hydrogel was stuck on the thumb and the two sections were connected with wires to obtain a hydrogel strain sensor. Correspondingly, as the finger bends, the hydrogel bends and stretches. Not only bending reduces the volume of pores inside the hydrogel, but stretching also makes the hydrogel longer, which causes the resistance of the hydrogel to become higher with the bending angle. Therefore, the hydrogel can be used as the strain sensor to detect hand movement. We attached the hydrogel strain sensor to the thumb and swiped the screen of the phone to browse the web ordinary, as shown in Fig. 9(a) and (b). Fig. 9(c) shows the hydrogel during the process of sliding the mobile phone and Fig. 9(d) shows the corresponding resistance change rate of the hydrogel during this process. In the initial state, the thumb and the hydrogel are located above the screen. Then, the finger bends toward the bottom side of the mobile phone screen, and the hydrogel also bends at about 90°. The resistance of the

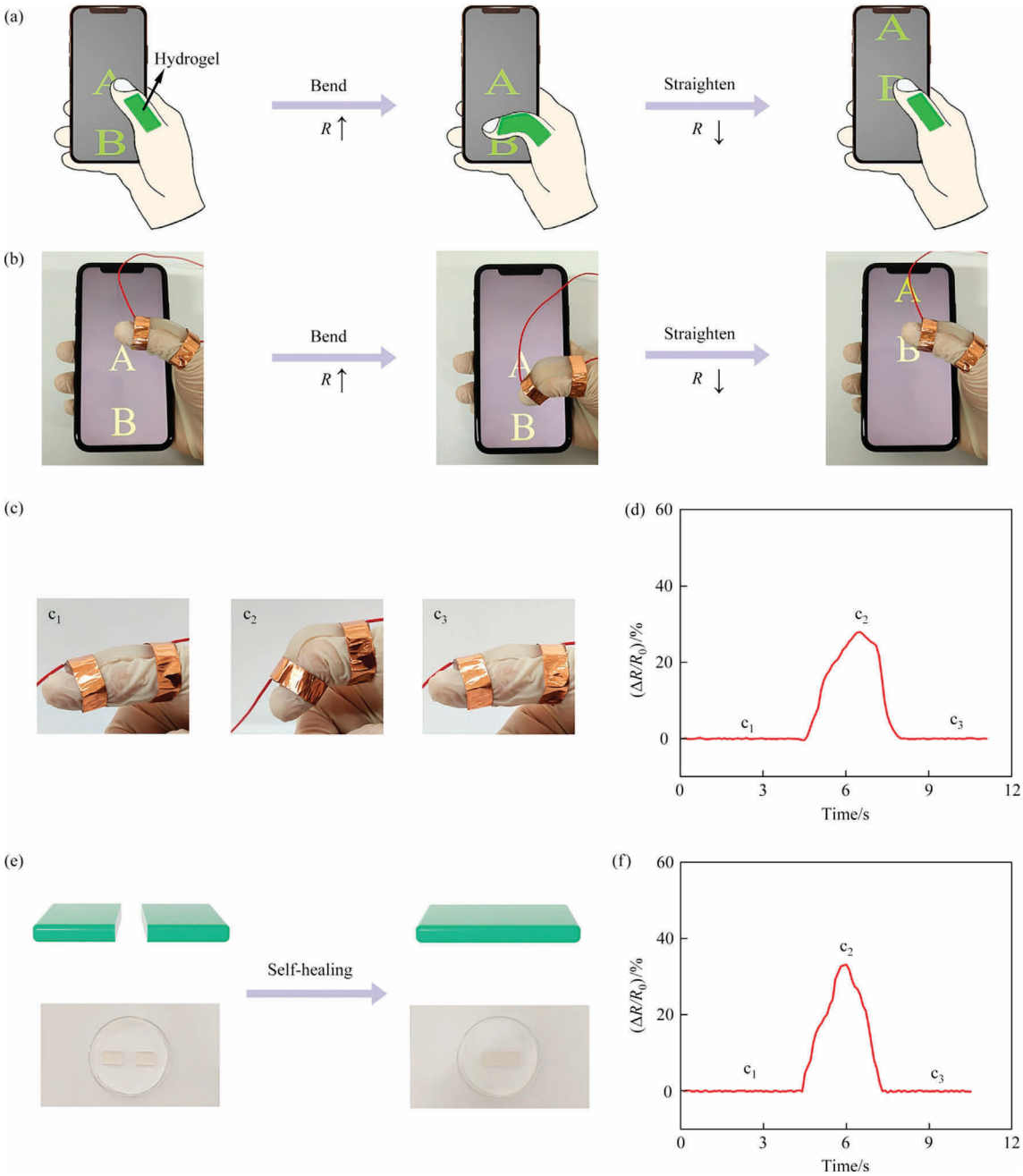

Fig. 9. (a) Schematic illustration of the hydrogel serving as the strain sensor. (b) Photographs of the hydrogel serving as the strain sensor. (c) Photographs of the hydrogel during the process of sliding the mobile phone. (c_1: initial state of the strain sensor, c_2: bent state of the strain sensor, c_3: straightened state of the strain sensor.) (d) Resistance change rate of the hydrogel during the process of sliding the mobile phone screen by thumb finger. (e) Self-healing property of the strain sensor. (f) Resistance change rate of the hydrogel during the process of sliding the mobile phone screen by thumb finger after self-healing.

hydrogel continues to increase toward the maximum value when it is bent to the maximum angle during this process. Finally, the finger touches the screen and swipes up to return to the initial state, whereas the hydrogel also bends back to the position at 0°. The resistance of the hydrogel continues to decrease toward initial value during this process. Although two bending processes last about 3 s in total, the hydrogel still clearly shows the resistance change during the process. Moreover, the hydrogel could continue to monitor the finger movement serving as the strain sensor after self-healing, as shown in Fig. 9(e) and (f). Consequently, the hydrogel has the potential for wearable self-healing sensor applications.

4. Conclusions

We have designed and fabricated a self-healing conductive ionic hydrogel containing OSA, CMC, AGO, and Li^+ for flexible sensors. The presence of Schiff base structure and Li^+ provides both good self-healing and conductive properties. Through comparative experiments, we have found that the introduction of AGO improves the mechanical properties of the hydrogel. The hydrogel can be used as the conductive material to light up the LED strip, and after cutting and healing, it still exhibits excellent electrical conductivity. Additionally, the conductivity of the hydrogel can change under bending or compression conditions. As such, the hydrogel can be used not only as the pressure sensor to record and transmit the information of pressed Morse code through the resistance changes, but also as the strain sensor to monitor sliding movement of thumb finger to browse the web with the mobile phone. Results show that the OSA-CMC-AGO/Li^+ hydrogel may have potential applications in wearable electronic devices as the flexible sensors.

Data Availability

The data that has been used is confidential.

Declaration of Competing Interest

The authors declare that they have no known competing financial interests or personal relationships that could have appeared to influence the work reported in this paper.

Acknowledgements

This work was granted financial support from National Natural Science Foundation of China (51873009) and Beijing Natural Science Foundation (2192042).

Supplementary Material

Supplementary data to this article can be found online at https://doi.org/10.1016/j.cjche.2022.02.022.

References

[1] J.Y. Nie, B.Y. Pei, Z.K. Wang, Q.L. Hu, Construction of ordered structure in polysaccharide hydrogel: A review, *Carbohydr. Polym.* 205 (2019) 225–235.
[2] Y. Cheng, K. Ren, C. Huang, J. Wei, Self-healing graphene oxide-based nanocomposite hydrogels serve as near-infrared light-driven valves, *Sens. Actuat. B Chem.* 298 (2019) 126908.
[3] Y. Cheng, K. Ren, D. Yang, J. Wei, Bilayer-type fluorescence hydrogels with intelligent response serve as temperature/pH driven soft actuators, *Sens. Actuat. B Chem.* 255 (2018) 3117–3126.
[4] C. Huang, Y. Cheng, Z.W. Gao, H.B. Zhang, J. Wei, Portable label-free inverse opal photonic hydrogel particles serve as facile pesticides colorimetric monitoring, *Sens. Actuat. B Chem.* 273 (2018) 1705–1712.
[5] V. Yesilyurt, M.J. Webber, E.A. Appel, C. Godwin, R. Langer, D.G. Anderson, Injectable self-healing glucose-responsive hydrogels with pH-regulated mechanical properties, *Adv. Mater.* 28 (1) (2016) 86–91.
[6] Y.F. Wang, Z.H. Chen, N.S. Li, H.B. Zhang, J. Wei, Programmable photo-responsive self-healing hydrogels for optical information coding and encryption, *Eur. Polym. J.* 166 (2022) 111025.
[7] Y.S. Li, X. Wang, Y. Wei, L. Tao, Chitosan-based self-healing hydrogel for bioapplications, *Chin. Chem. Lett.* 28 (11) (2017) 2053–2057.
[8] Z.Y. Liu, Y. Wang, Y.Y. Ren, G.Q. Jin, C.C. Zhang, W. Chen, F. Yan, Poly(ionic liquid) hydrogel-based anti-freezing ionic skin for a soft robotic gripper, *Mater. Horiz.* 7 (3) (2020) 919–927.
[9] Y. Cheng, C. Huang, D. Yang, K. Ren, J. Wei, Bilayer hydrogel mixed composites that respond to multiple stimuli for environmental sensing and underwater actuation, *J. Mater. Chem. B* 6 (48) (2018) 8170–8179.
[10] J.J. Wang, Q. Zhang, X.X. Ji, L.B. Liu, Highly stretchable, compressible, adhesive, conductive self-healing composite hydrogels with sensor capacity, *Chin. J. Polym. Sci.* 38 (11) (2020) 1221–1229.
[11] K. Ren, Y. Cheng, C. Huang, R. Chen, Z. Wang, J. Wei, Self-healing conductive hydrogels based on alginate, gelatin and polypyrrole serve as a repairable circuit and a mechanical sensor, *J. Mater. Chem. B* 7 (37) (2019) 5704–5712.
[12] Q.B. Guan, G.H. Lin, Y.Z. Gong, J.F. Wang, W.Y. Tan, D.Q. Bao, Y.N. Liu, Z.W. You, X.H. Sun, Z. Wen, Y. Pan, Highly efficient self-healable and dual responsive hydrogel-based deformable triboelectric nanogenerators for wearable electronics, *J. Mater. Chem. A* 7 (23) (2019) 13948–13955.
[13] Y.T. Wang, Q. Chang, R.X. Zhan, K.G. Xu, Y. Wang, X.Y. Zhang, B.Y. Li, G.X. Luo, M. Xing, W. Zhong, Tough but self-healing and 3D printable hydrogels for E-skin, E-noses and laser controlled actuators, *J. Mater. Chem. A* 7 (43) (2019) 24814–24829.
[14] V.K. Rao, N. Shauloff, X.M. Sui, H.D. Wagner, R. Jelinek, Polydiacetylene hydrogel self-healing capacitive strain sensor, *J. Mater. Chem. C* 8 (18) (2020) 6034–6041.
[15] C. Jiang, Y.S. Li, H. Wang, D.S. Chen, Y.Q. Wen, A portable visual capillary sensor based on functional DNA crosslinked hydrogel for point-of-care detection of lead ion, *Sens. Actuat. B Chem.* 307 (2020) 127625.
[16] W. Li, C. Jiang, S. Lu, F. Wang, Z.J. Zhang, T.W. Wei, Y.H. Chen, J. Qiang, Z.Y. Yu, X.Q. Chen, A hydrogel microsphere-based sensor for dual and highly selective detection of Al^{3+} and Hg^{2+}, *Sens. Actuat. B Chem.* 321 (2020) 128490.
[17] X.B. Ma, R. Yang, K.P.C. Sekhar, B. Chi, Injectable hyaluronic acid/poly(γ-glutamic acid) hydrogel with step-by-step tunable properties for soft tissue engineering, *Chin. J. Polym. Sci.* 39 (8) (2021) 957–965.
[18] C.J. Liu, X.L. Guo, C.P. Ruan, H.L. Hu, B.P. Jiang, H. Liang, X.C. Shen, An injectable thermosensitive photothermal-network hydrogel for near-infrared-triggered drug delivery and synergistic photothermal-chemotherapy, *Acta Biomater.* 96 (2019) 281–294.
[19] F.Y. Ding, S.P. Wu, S.S. Wang, Y. Xiong, Y. Li, B. Li, H.B. Deng, Y.M. Du, L. Xiao, X. W. Shi, A dynamic and self-crosslinked polysaccharide hydrogel with autonomous self-healing ability, *Soft Matter* 11 (20) (2015) 3971–3976.
[20] Y. Liu, L.J. Duan, M.J. Kim, J.H. Kim, D.J. Chung, *In situ* sodium alginate-hyaluronic acid hydrogel coating method for clinical applications, *Macromol. Res.* 22 (3) (2014) 240–247.
[21] Y.Q. Wang, Y.N. Xue, S.R. Li, X.H. Zhang, H.X. Fei, X.G. Wu, S.B. Sang, X.N. Li, M. Wei, W.Y. Chen, Nanocomposite carbon dots/PAM fluorescent hydrogels and their mechanical properties, *J. Polym. Res.* 24 (12) (2017) 1–7.
[22] P. Reutenauer, E. Buhler, P.J. Boul, S.J. Candau, J.M. Lehn, Room temperature dynamic polymers based on Diels-Alder chemistry, *Chemistry* 15 (8) (2009) 1893–1900.
[23] W.W. Hou, N.N. Sheng, X.H. Zhang, Z.H. Luan, P.F. Qi, M. Lin, Y.Q. Tan, Y.Z. Xia, Y.H. Li, K.Y. Sui, Design of injectable agar/NaCl/polyacrylamide ionic hydrogels for high performance strain sensors, *Carbohydr. Polym.* 211 (2019) 322–328.
[24] K. Lei, Z. Li, D.D. Zhu, C.Y. Sun, Y.L. Sun, C.C. Yang, Z. Zheng, X.L. Wang, Polysaccharide-based recoverable double-network hydrogel with high strength and self-healing properties, *J. Mater. Chem. B* 8 (4) (2020) 794–802.
[25] M. Wu, B. Johannesson, M. Geiker, A review: Self-healing in cementitious materials and engineered cementitious composite as a self-healing material, *Constr. Build. Mater.* 28 (1) (2012) 571–583.
[26] Y. Yang, M.W. Urban, Self-healing polymeric materials, *Chem. Soc. Rev.* 42 (17) (2013) 7446.
[27] H.L. Huang, G. Ye, C.X. Qian, E. Schlangen, Self-healing in cementitious materials: Materials, methods and service conditions, *Mater. Des.* 92 (2016) 499–511.
[28] H.L. Qin, T. Zhang, N. Li, H.P. Cong, S.H. Yu, Anisotropic and self-healing hydrogels with multi-responsive actuating capability, *Nat. Commun.* 10 (1) (2019) 2202.
[29] M.M. Kang, S.L. Liu, O. Oderinde, F. Yao, G.D. Fu, Z.H. Zhang, Template method for dual network self-healing hydrogel with conductive property, *Mater. Des.* 148 (2018) 96–103.
[30] M. Roberts, M. Hanson, A. Massey, E. Karren, P. Kiser, Dynamically restructuring hydrogel networks formed with reversible covalent crosslinks, *Adv. Mater.* 19 (18) (2007) 2503–2507.
[31] L. Saunders, P.X. Ma, Self-healing supramolecular hydrogels for tissue engineering applications, *Macromol. Biosci.* 19 (1) (2019) e1800313.
[32] S.Z. Li, M.J. Pei, T.T. Wan, H.J. Yang, S.J. Gu, Y.Z. Tao, X. Liu, Y.S. Zhou, W.L. Xu, P. Xiao, Self-healing hyaluronic acid hydrogels based on dynamic Schiff base linkages as biomaterials, *Carbohydr. Polym.* 250 (2020) 116922.
[33] Z. Wei, J.H. Yang, Z.Q. Liu, F. Xu, J.X. Zhou, M. Zrínyi, Y. Osada, Y.M. Chen, Novel biocompatible polysaccharide-based self-healing hydrogel, *Adv. Funct. Mater.* 25 (9) (2015) 1352–1359.

[34] J. Xu, D.G. Yang, W.J. Li, Y. Gao, H.B. Chen, H.M. Li, Phenylboronate-diol crosslinked polymer gels with reversible sol-gel transition, *Polymer* 52 (19) (2011) 4268–4276.
[35] X. Zhang, S.T. Jiang, T.F. Yan, X.T. Fan, F. Li, X.D. Yang, B. Ren, J.Y. Xu, J.Q. Liu, Injectable and fast self-healing protein hydrogels, *Soft Matter* 15 (38) (2019) 7583–7589.
[36] Z. Wei, J.H. Yang, X.J. Du, F. Xu, M. Zrinyi, Y. Osada, F. Li, Y.M. Chen, Dextran-based self-healing hydrogels formed by reversible Diels-alder reaction under physiological conditions, *Macromol. Rapid Commun.* 34 (18) (2013) 1464–1470.
[37] H.J. Zhang, H.S. Xia, Y. Zhao, Poly(vinyl alcohol) Hydrogel Can Autonomously Self-Heal, *ACS Macro Lett.* 1 (11) (2012) 1233–1236.
[38] I. Hussain, S.M. Sayed, S.L. Liu, O. Oderinde, F. Yao, G.D. Fu, Glycogen-based self-healing hydrogels with ultra-stretchable, flexible, and enhanced mechanical properties *via* sacrificial bond interactions, *Int. J. Biol. Macromol.* 117 (2018) 648–658.
[39] D.L. Zhao, Q. Tang, Q. Zhou, K. Peng, H.Y. Yang, X.Y. Zhang, A photo-degradable injectable self-healing hydrogel based on star poly(ethylene glycol)-*b*-polypeptide as a potential pharmaceuticals delivery carrier, *Soft Matter* 14 (36) (2018) 7420–7428.
[40] Y.X. Liu, M. Zhou, Y. Liu, X. Han, X.Z. Zhang, S.M. Liu, Host-guest interaction-mediated fabrication of aggregation-induced emission supramolecular hydrogel for use as aqueous light-harvesting systems, *Supramol. Chem.* 32 (8) (2020) 445–451.
[41] F.Y. Ding, X.W. Shi, S. Wu, X.H. Liu, H.B. Deng, Y.M. Du, H.B. Li, Flexible polysaccharide hydrogel with pH-regulated recovery of self-healing and mechanical properties, *Macromol. Mater. Eng.* 302 (11) (2017) 1700221.
[42] S.Q. Chang, B.X. Wang, Y.Z. Liu, Z. Li, X.D. Hu, X.H. Zhang, H.Q. Zhang, Radiation-assistant preparation of highly conductive, transparent and self-healing hydrogels with triple-network structure, *Polymer* 188 (2020) 122156.
[43] B. Guo, Z. Ma, L.J. Pan, Y. Shi, Properties of conductive polymer hydrogels and their application in sensors, *J. Polym. Sci. B Polym. Phys.* 57 (23) (2019) 1606–1621.
[44] Q.F. Rong, W.W. Lei, M.J. Liu, Conductive hydrogels as smart materials for flexible electronic devices, *Chemistry* 24 (64) (2018) 16930–16943.
[45] J.J. Yin, Q.Q. Liu, J.X. Zhou, L.X. Zhang, Q.R. Zhang, R.D. Rao, S.F. Liu, T.F. Jiao, Self-assembled functional components-doped conductive polypyrrole composite hydrogels with enhanced electrochemical performances, *RSC Adv.* 10 (18) (2020) 10546–10551.
[46] H. Peng, Y.Y. Lv, G.G. Wei, J.Z. Zhou, X.J. Gao, K.J. Sun, G.F. Ma, Z.Q. Lei, A flexible and self-healing hydrogel electrolyte for smart supercapacitor, *J. Power Sources* 431 (2019) 210–219.
[47] P. Chakraborty, T. Guterman, N. Adadi, M. Yadid, T. Brosh, L. Adler-Abramovich, T. Dvir, E. Gazit, A self-healing, all-organic, conducting, composite peptide hydrogel as pressure sensor and electrogenic cell soft substrate, *ACS Nano* 13 (1) (2019) 163–175.
[48] M. Ginting, S.P. Pasaribu, I. Masmur, J. Kaban, Hestina, Self-healing composite hydrogel with antibacterial and reversible restorability conductive properties, *RSC Adv.* 10 (9) (2020) 5050–5057.
[49] S. Pairatwachapun, N. Paradee, A. Sirivat, Controlled release of acetylsalicylic acid from polythiophene/carrageenan hydrogel *via* electrical stimulation, *Carbohydr. Polym.* 137 (2016) 214–221.
[50] A.R. Spencer, A. Primbetova, A.N. Koppes, R.A. Koppes, H. Fenniri, N. Annabi, Electroconductive gelatin methacryloyl-PEDOT: PSS composite hydrogels: Design, synthesis, and properties, *ACS Biomater. Sci. Eng.* 4 (5) (2018) 1558–1567.
[51] T. Nezakati, A. Seifalian, A. Tan, A.M. Seifalian, Conductive polymers: Opportunities and challenges in biomedical applications, *Chem. Rev.* 118 (14) (2018) 6766–6843.
[52] L.P. Yue, X.Y. Zhang, W.D. Li, Y. Tang, Y.P. Bai, Quickly self-healing hydrogel at room temperature with high conductivity synthesized through simple free radical polymerization, *J. Appl. Polym. Sci.* 136 (18) (2019) 47379.
[53] Z.H. Qin, X. Sun, Q.Y. Yu, H.T. Zhang, X.J. Wu, M.M. Yao, W.W. Liu, F.L. Yao, J.J. Li, Carbon nanotubes/hydrophobically associated hydrogels as ultrastretchable, highly sensitive, stable strain, and pressure sensors, *ACS Appl. Mater. Interfaces* 12 (4) (2020) 4944–4953.
[54] C. Lim, Y. Shin, J. Jung, J.H. Kim, S. Lee, D.H. Kim, Stretchable conductive nanocomposite based on alginate hydrogel and silver nanowires for wearable electronics, *APL Mater.* 7 (3) (2018) 031502.
[55] J.Q. Zhang, L.J. Wan, Y. Gao, X.L. Fang, T. Lu, L.K. Pan, F.Z. Xuan, Highly stretchable and self-healable MXene/polyvinyl alcohol hydrogel electrode for wearable capacitive electronic skin, *Adv. Electron. Mater.* 5 (7) (2019) 1900285.
[56] B.G. Li, C. Wu, C.Y. Wang, Z.Y. Luo, J.P. Cao, Fabrication of tough, self-recoverable, and electrically conductive hydrogels by *in situ* reduction of poly (acrylic acid) grafted graphene oxide in polyacrylamide hydrogel matrix, *J. Appl. Polym. Sci.* 137 (23) (2020) 48781.
[57] S.J. Peng, X.Z. Jiang, X.T. Xiang, K. Chen, G.Q. Chen, X.C. Jiang, L.X. Hou, High-performance and flexible solid-state supercapacitors based on high toughness and thermoplastic poly(vinyl alcohol)/NaCl/glycerol supramolecular gel polymer electrolyte, *Electrochim. Acta* 324 (2019) 134874.
[58] J.J. Li, H.L. Wei, Y. Peng, L.F. Geng, L.M. Zhu, X.Y. Cao, C.S. Liu, H. Pang, A multifunctional self-healing G-P_yB/KCl hydrogel: Smart conductive, rapid room-temperature phase-selective gelation, and ultrasensitive detection of alpha-fetoprotein, *Chem. Commun.* 55 (55) (2019) 7922–7925.
[59] L.Y. Fang, Z.F. Cai, Z.Q. Ding, T.Y. Chen, J.C. Zhang, F.B. Chen, J.Y. Shen, F. Chen, R. Li, X.C. Zhou, Z. Xie, Skin-inspired surface-microstructured tough hydrogel electrolytes for stretchable supercapacitors, *ACS Appl. Mater. Interfaces* 11 (24) (2019) 21895–21903.
[60] B.W. Yang, W.Z. Yuan, Highly stretchable and transparent double-network hydrogel ionic conductors as flexible thermal-mechanical dual sensors and electroluminescent devices, *ACS Appl. Mater. Interfaces* 11 (18) (2019) 16765–16775.
[61] S.J. Han, C.R. Liu, X.Y. Lin, J.W. Zheng, J. Wu, C. Liu, Dual conductive network hydrogel for a highly conductive, self-healing, anti-freezing, and non-drying strain sensor, *ACS Appl. Polym. Mater.* 2 (2) (2020) 996–1005.
[62] Q.H. Wang, X.F. Pan, J.J. Guo, L.L. Huang, L.H. Chen, X.J. Ma, S.L. Cao, Y.H. Ni, Lignin and cellulose derivatives-induced hydrogel with asymmetrical adhesion, strength, and electriferous properties for wearable bioelectrodes and self-powered sensors, *Chem. Eng. J.* 414 (2021) 128903.
[63] W.H. Zheng, Y.Y. Li, L.J. Xu, Y.D. Huang, Z.X. Jiang, B. Li, Highly stretchable, healable, sensitive double-network conductive hydrogel for wearable sensor, *Polymer* 211 (2020) 123095.